Finite Element Analysis and Optimization Design of Combined Vehicle Suspension Girder Lateral Stabilizer Bar Bushing

ZHU Yinan[1, a *], GENG Daoshuang[2, b], LI Nawen[1, c]

[1]Guangxi Key Laboratory of Information Materials, Guilin University of Electronic Technology, Guilin, Guangxi 541004, P.R. China
[2]School of Mechanical Electrical Engineering, Guilin University of Electronic Technology, Guilin, Guangxi 541004, P.R. China

[a]*372738211@qq.com, [b]1094861305@qq.com, [c]182252503@qq.com

Abstract. The stabilizer bar bushing as one of the most important parts of the automobile shock absorber, because of its complex structure using the rubber, and the rubber has nonlinearity and incompressibility, therefore using traditional numerical analysis method optimization calculation is very difficult. With the rapid development of the rapid development of computer aided engineering and finite element method, the numerical analysis technique to solve the mechanical problems of rubber materials becomes possible. This paper mainly introduces the ABAQUS finite element analysis software for vehicle rubber elastic element stiffness analysis and optimization design process, using Mooney-Rivlin equation, four kinds of design model of assembly interference and three directions static stiffness analysis, and then according to the stress strain results were optimized, we design a mechanical structure is the better performance of the liner model. The results show that the finite element analysis technology optimization of stabilizer bar bushing design method is feasible.

Introduction

Modern cars in order to improve the ride comfort, which suspensions are generally more soft, and the normal work of the suspension system in addition to need to have good damping effect of springs and dampers, and also need to lateral stability of the outstanding performance of the auxiliary rod, because the spring and shock absorber is only responsible for car wheel control. However, front and rear stabilizer bar is responsible for coordination of the suspension system. In the car through the corners due to the centrifugal force, lateral suspension is compressed, inboard suspension subjected to tension, causing the vehicle big lateral tilt, seriously affected the stability of the vehicle control, in order to reduce the tilt, and improve driving safety and need to in car installed with transverse stable rod. The motion state of the horizontal stabilizer bar must have the following basic characteristics: good wear resistance and aging resistance, ozone resistance, low temperature brittleness, noise reduction, long life and so on. Transverse stabilizer bar bushing is currently used in rubber materials, with the car and the road sediment, dust of the invasion, the rubber body itself will cause permanent deformation and wear, the overall performance products will decrease, triggered by the noise and friction lining failure, will be the vehicle to use the common problems in the process, in order to solve the adverse effects, many scholars and engineers began new combined structure of automobile suspension transverse stability rod bushing synchronous development work.

For the research of bushing, Litwin [1] has been developed for the lubrication of the bearing bush, and verify that the traditional liner model is not consistent with hydrodynamic lubrication. Zhukov [2] in the framework of nonlinear mechanics, rigid support between an elastomeric bushing longitudinal shear and torsion of the examples to study torsional dependence of strain relationship can be double potential of longitudinal shear stiffness and longitudinal shear stiffness. Tan, et al. [3] To overcome the increase in the unsprung mass and deformation of the magnet gap for in-wheel-motor-propelling

systems, a novel topology scheme had been presented in previous work, an optimal matching design between the suspension and the rubber bushing is employed for the novel system to reduce the effect of the road surface roughness on the magnet gap as much as possible, on the basis of good ride quality and comfort. Han, et al. [4] Design a kind of viscoelastic hysteresis of the rubber material often causes thermal failure of PDM (Positive Displacement Motor) stator bushing. Lindberg, et al. [5] A rubber bushing model for noise reduction and vibration reduction is designed, and a very good vibration reduction effect is achieved. Kaya [6] design of stabilizer bar bushing using the integral algorithm is optimized, and has achieved satisfactory results. Puel, et al. [7] Using parameter identification of nonlinear time-dependent rubber bushings models towards their integration in multibody simulations of a vehicle chassis. Zimmermann, et al. [8]. Used the finite element analysis technology to simulate the elastic modulus of the natural rubber, and provided the engineering support for the design of the bushing. Blom, et al. [9]. Have presented a dynamic torsional stiffness model of a magneto-sensitive circular annular rubber bushing where influences of frequency, amplitude and magnetic field dependence are included. A cylindrical rubber bushing was designed by Tupholme [10], and the radial stiffness of the rubber bushing was analyzed. Advanced modular modeling and Simulation of automotive rubber bushing using dynamic mechanical model by Sedlaczek, et al [11]. Cerit et al. [12] Study on the influence of the stress distribution and fatigue property of rubber bushing, in this research, anti-roll bars used in ground vehicle to reduce body roll by resisting any uneven vertical motion between the pair of wheels suffer from fatigue failure.

In this paper, we using the finite element software ABAQUS on the static stiffness analysis of bushing, respectively from different directions of the stabilizer bar bushing radial and assembly process simulation obtains the corresponding radial force - displacement nephogram and assembly cloud chart, and use it as a reference, the stabilizer bar bushing for the overall design and satisfactory results are obtained.

Basic Theory and Experimental Method of Elastic Properties of Rubber Components

The Determination of the Expression of the Strain Energy Function. Prior to the finite element analysis of the rubber products, we should first understand the characteristics of the rubber material and the constitutive equation, and input the experimental parameters into the finite element software to carry out the material setting. Rubber properties are very complex, it is very difficult to determine their nonlinear characteristics, cannot be used as a metal with quite a few parameters (such as elastic modulus and Poisson's ratio) to be described. In terms of material properties and geometrical properties, the rubber is a non-linear non compressible material (Poisson's ratio between 0.45-0.5). Many people at home and abroad put forward their own opinions on the test methods and constitutive equations of rubber, but it is still difficult to determine a very effective solution to the equation. Therefore there are many kinds of strain energy function in the description of the mechanical properties of rubber materials. At present, most of the use of constitutive equations is the Mooney-Rivlin model proposed by Rivlin in 1976, and the Hookean - Neo model proposed by Pence et al [13]. This paper uses the Mooney-Rivlin model.

The expression of strain energy function of Mooney-Rivlin polynomial is [14]:

$$W = \sum_{i+j=1}^{N} C_{ij}(I_1 - 3)^i (I_2 - 3)^j + \frac{1}{2}K(\sqrt{I_3} - 1)^2 . \tag{1}$$

In the formula, W is the strain energy; C_{ij} is the material parameter, $i \leq 1$, $j \leq 1$, i and j are positive integers; I_1, I_2 and I_3 are one or two, three order Cauchy-Green strain tensor; K is the stretching length in three directions.

The relationship between I_1, I_2, I_3 and the three main stretching ratio λ_1, λ_2, λ_3 of the hyperelastic material is [15-17]:

$$I_1 = \lambda_1^2 + \lambda_2^2 + \lambda_3^3 \qquad (2)$$

$$I_2 = \lambda_1^2 \lambda_2^2 + \lambda_2^2 \lambda_3^2 + \lambda_3^2 \lambda_1^2 \qquad (3)$$

$$I_3 = (\lambda_1 \lambda_2 \lambda_3)^2 \qquad (4)$$

Because the rubber is a hyperelastic material, approximate incompressible, assuming that the material is completely incompressible [18-21], that is, when $I_3 = 1$, the expression of strain energy function in (1) can be changed into the next [22]:

$$W = C_{10}(I_1 - 3) + C_{01}(I_2 - 3) \qquad (5)$$

where, C_{10} and C_{01} are non-zero material coefficients, which can be obtained by uniaxial tensile test. However, in the actual testing process, this model is difficult to capture the stiffness caused by the extension of the hyperelastic material caused by the increase, therefore the Bederman model has been further improved [23]:

$$W = C_{10}(I_1 - 3) + C_{20}(I_1 - 3)^2 + C_{30}(I_1 - 3)^3 + C_{01}(I_2 - 3) \qquad (6)$$

In the formula, C_{10}, C_{20}, C_{30} and C_{01} are the material parameters, which can be obtained from uniaxial tensile test.

Experimental Test and Determination of Material Parameters. For the material parameters are obtained in the formula (4), there are two kinds of methods that are numerical calculation method and uniaxial tensile test method. This paper focuses on the uniaxial tensile test method. Usually a complete representation of the rubber hyperelastic material model theory, the laboratory needs three kinds of mechanical tests [24]: uniaxial tension (compression), biaxial tension (compression), plane shear. For the statics analysis of rubber products, uniaxial tension is one of the most easily and widely used in the construction of hyperelastic model, in this paper, the material properties of the finite element analysis, which is the single axis tensile test data, can be relatively accurate analysis results [25].

In order to obtain the state of pure tensile strain, the length of the specimen in the tensile direction is larger than that in the thickness direction. The purpose of this is to ensure that there is no restriction on the transverse direction of the specimen during the test. The size of dumbbell shaped specimen in experiments is: 31.4 ± 0.5 mm long, $6_0^{+0.4}$ mm wide, 2 ± 0.4 mm thick, the specimen standard using GB/T528. The tensile stress strain test of dumbbell shaped specimen is carried out on the electronic tensile test machine. Fig. 1 is a dumbbell shaped tensile samples two-dimensional map. Fig. 2 is a dumbbell sample finite element analysis model and deformation map, from the Fig. 2 we can see, due to the specimen is thin and soft material and deformation characteristics, experiment to pay attention to ensure that the dumbbell shape characteristics and rubber product material properties are consistent with the. Therefore, the recommended rate of uniaxial tensile test of super elastic material for 30~120mm/min.

Fig. 1 Dumbbell shaped standard tensile test specimen.

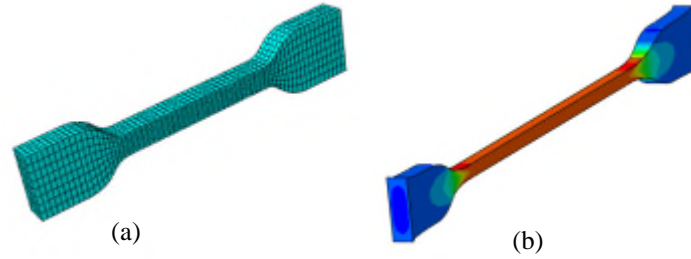<center>(a)</center>
<center>(b)</center>

Fig. 2 The finite element analysis model (a) and its deformation map (b) of the dumbbell specimen.

In the uniaxial tensile test of the electronic tensile machine, the strain and stress fitting curves of 30mm/min, 60mm/min and 120mm/min are respectively output, as shown in Fig. 3. We can clearly see the strain stress relationship at different rates, and the effect of loading rate on the relationship between stress and strain is negligible when the strain is 200%. The test data of three kinds of samples with single axial tension are shown in Table 1, which can be seen in the form of stress σ_i under different strain tension ratio [26].
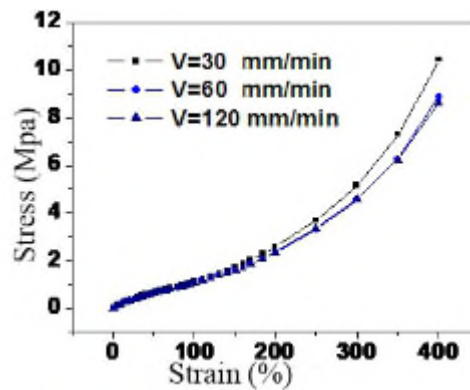

Fig. 3 The effect of loading rate on the tensile stress and strain of the dummy specimen and the fitting curve of strain stress test.

Table 1. Three rate uniaxial tensile strain-stress test values.

30mm/min		60mm/min		120mm/min	
Strain(%)	Stress	Strain(%)	Stress	Strain(%)	Stress
100	1.842	100	1.842	100	1.848
200	2.874	200	2.739	200	2.736
300	5.227	300	4.932	300	4.935
400	9.934	400	8.754	400	8.424

For incompressible rubber materials, in the special case of uniaxial tension, the strain energy function corresponding to the engineering stress calculation formula is:

$$\hat{\sigma}_1 = \frac{\partial W}{\partial \lambda_1} = \frac{\partial W}{\partial I_1}\frac{\partial I_1}{\partial \lambda_1} + \frac{\partial W}{\partial I_2}\frac{\partial I_2}{\partial \lambda_1} + \frac{\partial W}{\partial I_3}\frac{\partial I_3}{\partial \lambda_1}.$$

(7)

$$\hat{\sigma}_2 = \frac{\partial W}{\partial \lambda_2} = \frac{\partial W}{\partial I_1}\frac{\partial I_1}{\partial \lambda_2} + \frac{\partial W}{\partial I_2}\frac{\partial I_2}{\partial \lambda_2} + \frac{\partial W}{\partial I_3}\frac{\partial I_3}{\partial \lambda_2}.$$

(8)

$$\hat{\sigma}_3 = \frac{\partial W}{\partial \lambda_3} = \frac{\partial W}{\partial I_1}\frac{\partial I_1}{\partial \lambda_3} + \frac{\partial W}{\partial I_2}\frac{\partial I_2}{\partial \lambda_3} + \frac{\partial W}{\partial I_3}\frac{\partial I_3}{\partial \lambda_3}.$$

(9)

From the above three equations can be seen in the engineering stress and stretch ratio, the engineering error of stress and experimental values for [27-29]:

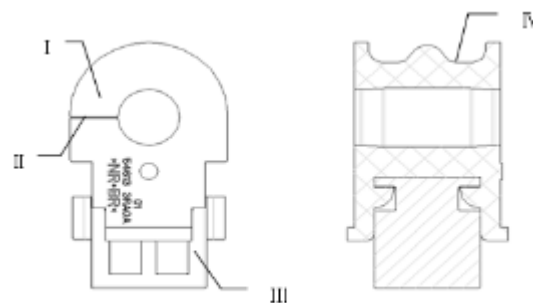$$S = \sum_{i=1}^{3} (\sigma_i - \hat{\sigma}_i)^2 \quad . \tag{10}$$

By the equation (10), it can be seen that using the least squares method, a set of material parameters C_{ij} can be found, making the error and S minimum, that is [30, 31]：

$$\frac{\partial S}{\partial C_{ij}} = 0 \quad . \tag{11}$$

With all of the above formula with the experimental results, and ultimately obtained material parameters: $C_{10} = 0.24$, $C_{01} = 0.043$, $C_{20} = 0.034$, $C_{30} = 0.0076$ were obtained. When ABAQUS is to be solved, they are import the software to solve the problem.

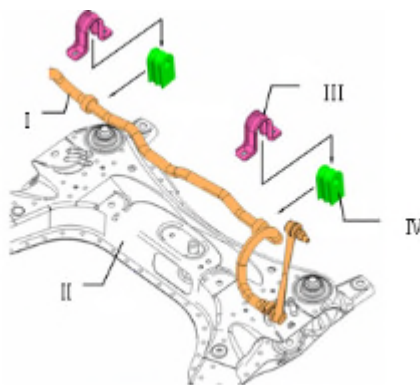**The New Combined Automobile Suspension Beam Stabilizer Bushing Model Establishment**

Beam Stabilizer Bar Bushing Structure Model Combined Vehicle Suspension. The product design feature is the selection of material is natural rubber, the design of the assembly with the guide groove plastic skeleton and rubber compound structure. The structure belongs to the domestic initiative, is characterized by anti-deformation, easy loading and unloading. By the use of the user authentication, the product can effectively reduce the friction noise, the lateral stability of the vehicle can play a better role in supporting the role of. The inner hole of the rubber part of the design for the two ends of the large middle small "drum" sealing structure, can prevent silt and dust from entering the stabilizer bar between the inner hole of the Bush and the gap, reduce wear and prolong the service life of the bush. The rubber material is added with the Plasthill7050 plasticizer which is compatible with the natural rubber, so that the lubricant in the formula is easy to migrate to the surface of the product, increase the lubricating property, reduce the friction, and eliminate the noise. Structure diagram shown in Fig. 4.

Ⅰ-Rubber body;　Ⅱ-The stabilizer bar assembly gap;　Ⅲ-Plastic skeleton;　Ⅳ-Clamp fixing groove
Fig. 4 Product structure diagram.

Product Design and Development Process. In the course of the development of the product development, according to the requirements of the quality system, we put development of the whole development process is divided into: the stage of product design and development, process design and development, product and process validation stages and mass production stage. This paper only considers the product design and development phase.

Product assembly drawing is shown in Fig. 5:

Ⅰ-Vehicle lateral stabilizer bar; Ⅱ-Sub-frame;   Ⅲ-Clamp; Ⅳ-Stabilizer bar bushing
Fig. 5 Sketch of the assembly of stable rod bushing.

In order to shorten the development cycle and save the cost of design, the project design process using numerical simulation technology, through the finite element analysis (FEA) of the product, can determine the different direction design of radial stiffness properties, interference and assembly improvement measures. In this paper, ABAQUS finite element analysis software is used to analyze the performance of the three directions of the product design. In the software, the rubber element is used in C3D8H, in order to improve the computer operation speed, the experimental fixture is simplified as a rigid body structure. In the analysis process, a stable force of 981 N is applied in the three directions.

According to the actual working condition of the stable rod bushing, the analysis process is divided into three processes:

(1) Interference fit. The stabilizing rod bushing and the shaft, the stabilizing rod bushing and the clamp are both interference fit, therefore, the influence of the prestressed on the product performance is considered before installation.
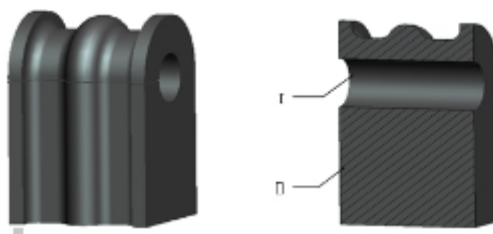
(2) Assembling. After the interference fit is completed, the flat plate and the clamp are tightened by bolts, so that the stable rod bushing is completely wrapped in the radial part.

(3) Radial analysis. Completed the interference fit and assembly, the bushing is wrapped with a strong prestressing force, and then calculate the stiffness of each direction required.

Product Finite Element Analysis and Optimization

The First Structure Design.

Design ideas.

I- The mating section of bushing Ⅱ- the supporting part of bushing
Fig. 6 The first structure design.

(1) The inner hole is designed for straight pass structure, after curing, the product is cut to facilitate the assembly of the stable rod bushing;

(2) Combined with the stabilizer bar bushing bearing direction, is designed structure on the lower end of the meat is thick, and the upper end of the meat is thin, and hence improve strength and also increases the elastic properties of the products;

(3) The design of slot type structure, prevent jump between the stabilizer bar bushing and clamp, to limit the role of clamp up;

(4) Using the poor compatibility of Plasthall 7050 plasticizer with natural rubber, the self - lubricating component in the formula is brought out to the surface of the product, which makes the surface of the product very lubrication, its greatly reduces the friction between the rubber parts and the metal rod. The first design structure is shown in Fig. 6.

ABAQUS simulation results.

For the first structure design, ABAQUS is used to simulate the interference fit and three directions-to-extrusion, and the results are shown in Fig. 7 and Fig. 8.
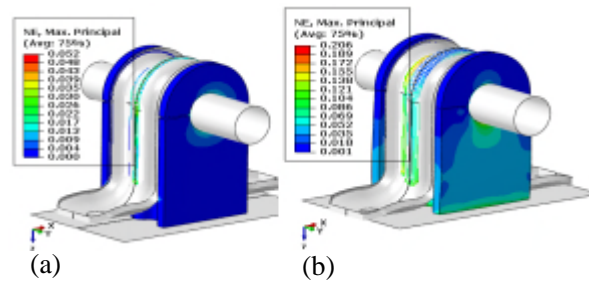
(a)   (b)

Fig. 7 Strain contour (a) after assembly of the stabilizer bar and Strain contour (b) after tightening of the clamp.

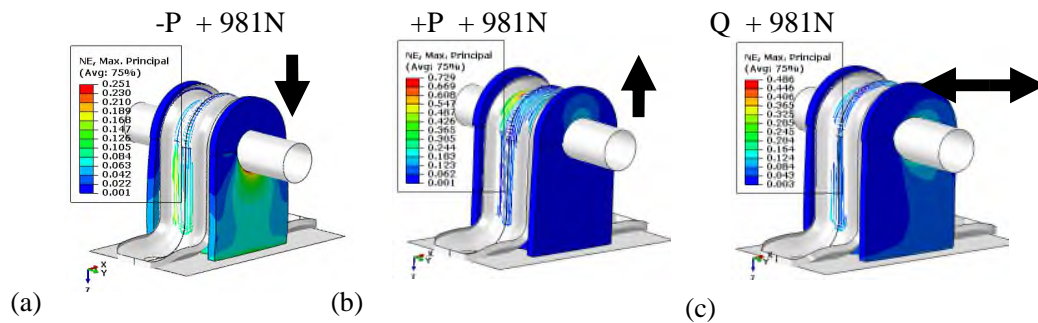-P + 981N   +P + 981N   Q + 981N

(a)   (b)   (c)

Fig. 8 -P direction strain contour map (a), +P direction strain contour map (b) and Q direction strain contour map (c).

In the process of finite element analysis and simulation, we are from the assembly interference, radial tension and compression in three aspects. From Fig. 7 and Fig. 8, we can see:

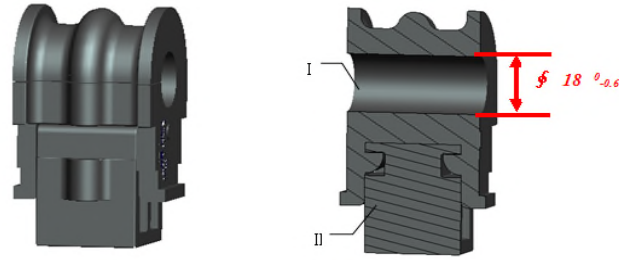(1) P, Q direction static stiffness is low, cannot meet the design requirements;

(2) Product resistance to permanent deformation ability is poor, lateral stable pole with rubber lining Suites lack of sustained tightening force, stable rod transverse jump move more likely, suspension control performance will be affected;

(3) Flesh of the bottom of the product, although the design enhance the elastic properties of the product, but the parts of the hardness is too large, affecting product overall use function.

Therefore, based on the theoretical analysis of the first product, we have carried out the second improvement to the product structure.

The Second Structural Improvement Design.

Improvement ideas. The lower end of the product bearing parts from a single rubber, changed to the rubber + plastic skeleton (PA66+ glass fiber) two components, and the two components separate processing, after their completed and then assembly. Because the PA66 has the advantages of high strength, excellent resilience, abrasion resistance, good damping effect, stable chemical properties and so on. The design results are shown in Fig. 9.

I- The mating section of bushing Ⅱ- the supporting part of bushing

Fig. 9 The second structure design.

ABAQUS simulation results. For the second structure design, ABAQUS is used to simulate the interference fit and three directions-to-extrusion, and the results are shown in Fig. 10 and Fig. 11.
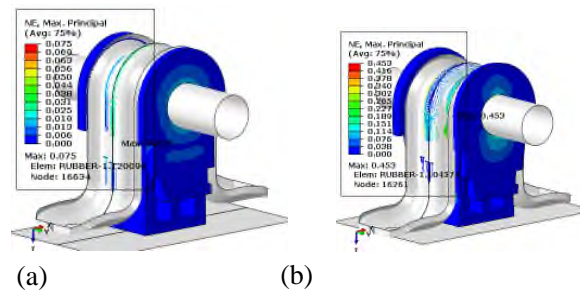

(a)   (b)

Fig. 10 Strain contour (a) after assembly of the stabilizer bar and Strain contour (b) after tightening of the clamp.

-P +981N   +P +981N   Q + 981N

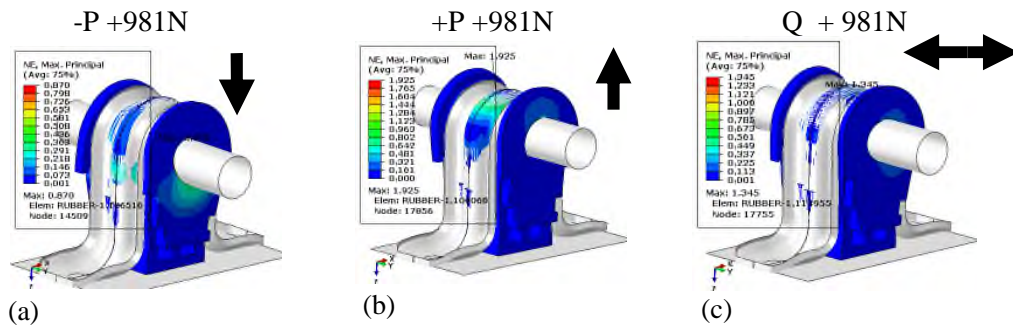(a)   (b)   (c)

Fig. 11 -P direction strain contour map (a), +P direction strain contour map (b) and Q direction strain contour map (c).

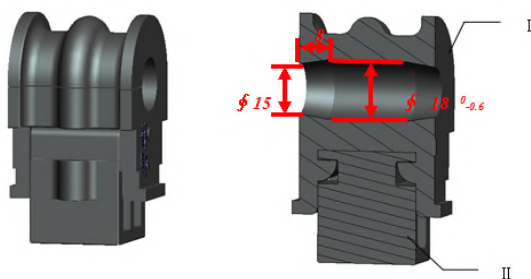From Fig. 10 and Fig. 11, we can see:

(1) P, Q direction static stiffness can meet the design requirements;

(2) The anti-deformation ability is greatly improved, the gap between the stable rod and the inner hole of the rubber bushing leads to excessive friction of the inner hole of the bushing, which influences the service life of the product.

Therefore, based on the theoretical analysis of the second product, we have carried out the third improved scheme to the product structure.

The Third Structural Improvement Design.

Improvement ideas. The rubber products in the hole part of the design into large at two poles and little in the middle of "drum" seal structure, to prevent the two parts of the mutual friction, prolong the service life of the product. The design results are shown in Fig. 12.

I- The mating section of bushing Ⅱ - the supporting part of bushing
Fig. 12 The third structure design.

ABAQUS simulation results. For the third structure design, ABAQUS is used to simulate the interference fit and three directions-to-extrusion, and the results are shown in Fig. 13 and Fig. 14.
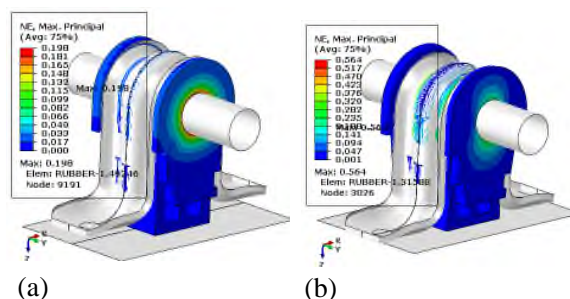

(a)   (b)

Fig. 13 Strain contour (a) after assembly of the stabilizer bar and Strain contour (b) after tightening of the clamp.

-P ＋981N   +P ＋981N   Q ＋981N

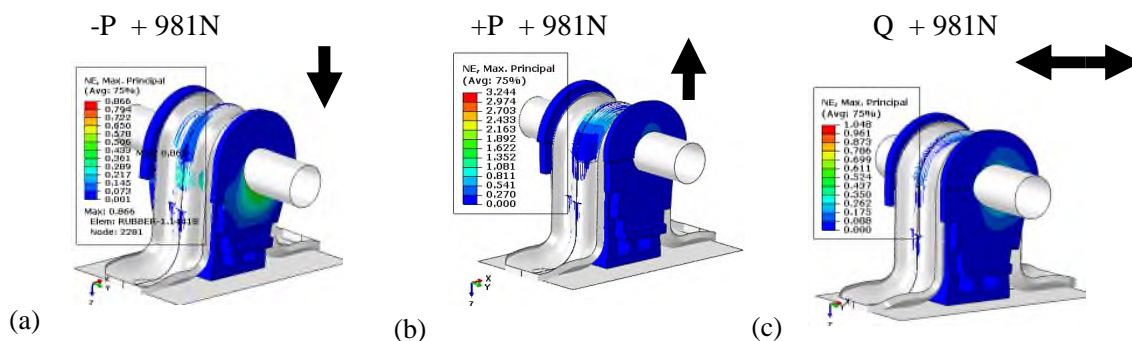(a)   (b)   (c)

Fig. 14 -P direction strain contour map (a), +P direction strain contour map (b) and Q direction strain contour map (c).
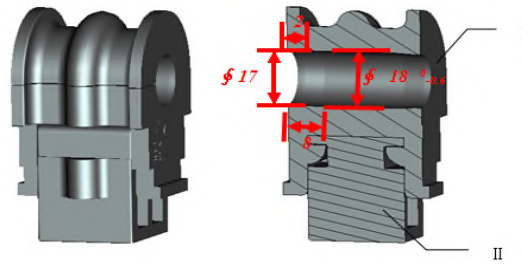
From Fig. 13 and Fig. 14, we can see:

The stability rod bushing assembly analysis is more difficult;

The friction of the inner hole of the stable rod bushing is improved, but the friction between the two ends of the part is still relatively large.

Therefore, based on the theoretical analysis of the third product, we have carried out the fourth improved scheme to the product structure.

The Fourth Structural Improvement Design.

Improvement ideas. Optimization of rubber inner hole "drum" seal structure to make it gradually smooth transition, in a decentralized assembly resistance reduce the stable rod bushing inner hole friction. The design results are shown in Fig. 15.

I- The mating section of bushing Ⅱ - the supporting part of bushing
Fig. 15 The fourth structure design.

ABAQUS simulation results. For the fourth structure design, ABAQUS is used to simulate the interference fit and three directions-to-extrusion, and the results are shown in Fig. 16 and Fig. 17.
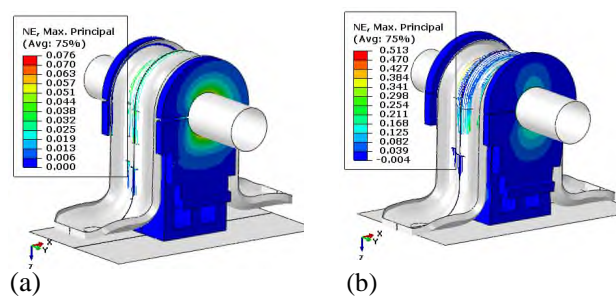

(a)   (b)

Fig. 16 Strain contour (a) after assembly of the stabilizer bar and Strain contour (b) after tightening of the clamp.

-P + 981N   +P + 981N   Q + 981N

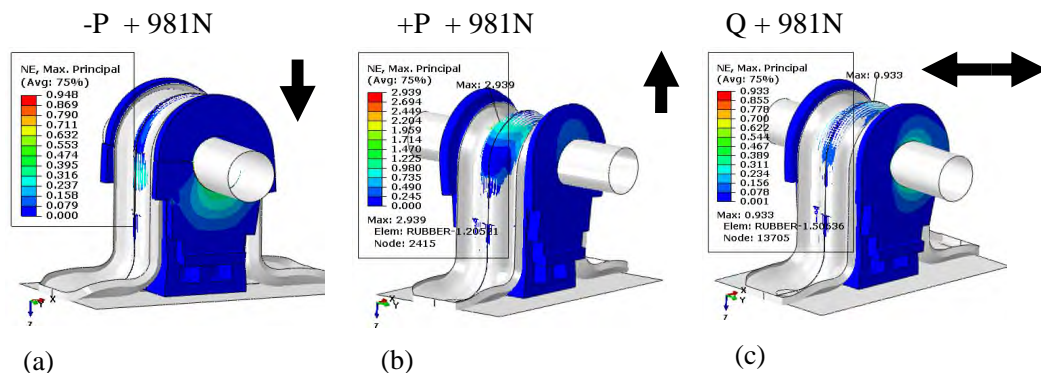

(a)   (b)   (c)

Fig. 17 -P direction strain contour map (a), +P direction strain contour map (b) and Q direction strain contour map (c).

From Fig. 16 and Fig. 17, we can see:

(1) P, Q direction static stiffness can meet the design requirements;

(2) The ability to resist deformation has been greatly improved;

(3) The situation of assembly difficulties has been improved, no excessive friction sliding.

Through the analysis of strain contrast (the relative change rate before and after applying force and deformation) can get the results of Table 2, the smaller displacement, the better anti fatigue performance, and the lower the stiffness.

Table 2. Comparative analysis of the results of the four schemes.

Step	Plan one	Plan two	Plan three	Plan four
Shrink fit	5.2%	7.5%	19.8%	7.6%
Assembly	20.6%	45.3%	56.4%	51.3%
+p quantity	25.1%	87.0%	86.6%	94.8%
-P quantity	72.9%	192.5%	324.4%	293.9%
Q quantity	40.6%	134.5%	104.8%	93.3%

Therefore, according to the requirements of product performance, processing production, assembly and use of comprehensive evaluation, the final product design and design of the structure is use the fourth state structures (as shown in Fig. 18)
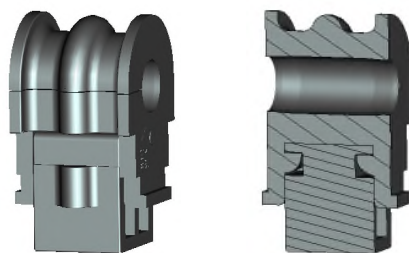

Fig. 18 Final shape structure diagram.

After test and found the fourth design is according to the engineering specifications and application requirements, not only radial stiffness meet the design needs, and assembly interference can also achieve good results, can be a good lock tight transverse stable rod to prevent the relative sliding and in the trial found that the qualified rate of the product has reached 97% and reached the preliminary planning of 95%, reduces the cost greatly, therefore, the fourth scheme is designed to meet the demand of the engineering.

Conclusion

To model combined vehicle suspension stabilizer bar bushing as the object of study, using ABAQUS software to calculate the radial force displacement characteristics and the too assembly interference are analyzed, and actual test results were compared. Results show that can meet the requirements of the project. The finite element analysis of the static stiffness of rubber has direct significance in engineering calculation. The analysis results of the static stress of the rubber stabilizer bar bushing can be used in the design and optimization of the whole structure. ABAQUS / CAE finite element analysis on the elastic properties of the rubber components is effective, and greatly reduce the products in the development of a number of trials, reduce the development cycle and cost, the method can be the overall structure of the new combination vehicle stabilizer bar bushing damper rubber is used in the design.

Acknowledgement

References

[1] W. Litwin, Properties comparison of rubber and three layer PTFE-NBR-bronze water lubricated bearings with lubricating grooves along entire bush circumference based on experimental tests, Tribol. Int. 90 (2015) 404-411.

[2] B. A. Zhukov, Nonlinear interaction of finite longitudinal shear with finite torsion of a rubber-like bushing, Mech. Solids 50(3) (2015) 337-344.

[3] D. Tan, C. Lu, C. B. Ren, Optimal matching between the suspension and the rubber bushing of the in-wheel motor system, P. I. Mech. Eng. D-J. Aut. 229(6) (2015) 758-769.

[4] C. J. Han, J. Zhang, Z. Liang, Thermal failure of rubber bushing of a Positive Displacement Motor: A study based on thermo-mechanical coupling, Appl. Therm. Eng. 67(1-2) (2014) 489-493.

[5] E. Lindberg, M. Ostberg, N. E. Horlin, et al., A vibro-acoustic reduced order model using undeformed coupling interface substructuring - application to rubber bushing isolation in vehicle suspension systems, Appl. Acoust. 78 (2014) 43-50.

[6] N. Kaya, Shape optimization of rubber bushing using differential evolution algorithm, Sci. World J. (2014) 379196.

[7] G. Puel, B. Bourgeteau, D. Aubry, Parameter identification of nonlinear time-dependent rubber bushings models towards their integration in multibody simulations of a vehicle chassis, Mech. Syst. Signal Pr. 36(2) (2013) 354-369.

[8] J. Zimmermann, M. Stommel, The mechanical behaviour of rubber under hydrostatic compression and the effect on the results of finite element analyses, Arch. Appl. Mech. 83(2) (2013) 293-302.

[9] P. Blom, L. Kari, The frequency, amplitude and magnetic field dependent torsional stiffness of a magneto-sensitive rubber bushing, Int. J. Mech. Sci. 60(1) (2012) 54-58.

[10] G. E. Tupholme, An analogy between radially-loaded rubber bush mountings and axially-loaded bonded rubber blocks, Mater. Design 32(10) (2011) 5038-5042.

[11] K. Sedlaczek, S. Dronka, J. Rauh, Advanced modular modelling of rubber bushings for vehicle simulations, Vehicle Syst. Dyn. 49(5) (2011) 741-759.

[12] M. Cerit, E. Nart, K. Genel, Investigation into effect of rubber bushing on stress distribution and fatigue behaviour of anti-roll bar, Eng. Fail. Anal. 17(5) (2010) 1019-1027.

[13] T. J. Pence, K. Gou, On compressible versions of the incompressible neo-Hookean material, Math. Mech. solids 20(2) (2015) 157-182.

[14] R. S. Rivlin, K. N. Sawyers, Strain-energy function for elastomers, Trans. Soc. Rheol. 20 (1976) 54557.

[15] Y. Zhou, Z. Q. Huang, L. Tan, et al., Cone bit bearing seal failure analysis based on the finite element analysis, Eng. Fail. Anal. 45 (2014) 292-299.

[16] M. C. Chen, X. C. Ping, W. H. Liu, et al., A novel hybrid finite element analysis of two polygonal holes in an infinite elastic plate, Eng. Fract. Mech. 83 (2012) 26-39.

[17] C. O. Horgan, The remarkable Gent constitutive model for hyperelastic materials, Int. J. Nonlin. Mech. 68 (2014) 9-16.

[18] K. Patra, R. K. Sahu, A visco-hyperelastic approach to modelling rate-dependent large deformation of a dielectric acrylic elastomer, Int. J. Mech. Mater. Des. 11(1) (2015) 79-90.

[19] W. Kin, H. Chung, M. Cho, Anisotropic hyperelastic modeling for face-centered cubic and diamond cubic structures, Comput. Method. Appl. M. 291(1) (2015) 216-239.

[20] S. Kundurthi, P. Mythravaruni, P. Ravindran, Vulcanization and the mechanical response of rubber, Z. Angew. Math. Phys. 66(3) (2015) 1109-1123.

[21] M. R. Mansouri, H. Darijani, Constitutive modeling of isotropic hyperelastic materials in an exponential framework using an elf-contained approach, Int. J. Solids and Struct. 51(25-26) (2014) 4316-4326.

[22] R. Osterlof, H. Wentzel, L. Kari, An efficient method for obtaining the hyperelastic properties of filled elastomers in finite strain applications, Polym. Test. 41 (2014) 44-54.

[23] K. Patra, R. K. Sahu, A visco-hyperelastic approach to modelling rate-dependent large deformation of a dielectric acrylic elastomer, Int. J. Mech. Mater. Des. 11(1) (2015) 79-90.

[24] C. Liu, C. M. Cady, M. L. Lovato, et al., Uniaxial tension of thin rubber liner sheets and hyperelastic model investigation, J. Mater. Sci. 50(3) (2015) 1401-1411.

[25] W. B. Shangguan, Z. H. Lu, Finite element analysis of elastic characteristics of rubber isolator for automotive powertrain systems, Chin. Intern. Combust. Engine Eng. 24(6) (2003) 50-55(in Chinese).

[26] A. Delattre, S. Lejeunes, S. Meo, et al., On the multiaxial amplitude-and frequency-dependent behavior of rubber: experiments and constitutive modeling, Rubber Chem. Technol. 87(3) (2014) 557-578.

[27] D. S. Dogan, A. Demirer, Determination of characteristics of natural rubber/styrene-butadiene rubber-based elastomer material filled with mica powder and glass spheres, J. Elastom. Plast. 47 (2015) 306-319.

[28] R. Rashetnia, S. Mohammadi, Finite strain fracture analysis using the extended finite element method with new set of enrichment functions, Int. J. Numer. Meth. Eng. 102(6) (2015) 1316-1351.

[29] H. B. Yang, F. Z. Li, T. W. Chan, et al., A simulation study on the effect of spring-shaped fillers on the vicoelasticity of rubber nanocomposite, Compos. Part B-Eng. 74(1) (2015) 171-177.

[30] B. Debbaut, A simple model for wire-reinforced polymer and rubber, Rheol. Acta 54(5) (2015) 403-409.

[31] N. Dehbari, J. C. Zhao, R. G. Peng, et al., Neutralisation and compatibilisation effects on novel water-swellable rubber composites, J. Mater. Sci. 50(15) (2015) 5157-5164.